European Journal of Computational Mechanics, 2015
Vol. 24, No. 1, 1–15, http://dx.doi.org/10.1080/17797179.2015.1012632

Taylor & Francis
Taylor & Francis Group

Effect of interface contact conditions on adaptive finite element simulation of sheet forming operations

Mohd Ahmed[a]*, Devender Singh[b] and Saiful Islam[a]

[a]*Engineering Faculty, Civil Engineering Department, K. K. University, Abha, Kingdom of Saudi Arabia;* [b]*Prasar Bharati, Delhi, India*

Interfacial contact can have significant influence on adaptive mesh refinement during finite element simulation of sheet forming process. In this work, effect of contact is examined on the adaptive simulation of deep drawing operations having different friction factor and thickness of sheets. The frictional contact at the die-blank interface in the sheet of various thicknesses is modelled in terms of a constant factor relating frictional stress to shear strength of the material. An h-adaptive technique has been employed for the refinement of mesh. A recovery-type error estimator based on the energy norm is used for guiding the h-refinement. Adaptively refined meshes obtained during simulation of the axisymmetric deep drawing operation using frictional and non-friction contact on different sheet thicknesses are presented and discussed.

Keywords: finite element analysis; adaptive refinement; adaptive simulation; sheet forming; contact conditions; deep drawing

1. Introduction

The classical improvement of finite element simulation accuracy using uniformly refined mesh throughout the domain is expensive and is not preferred in large-scale simulation. An adaptive technique that automatically searches the areas of insufficient accuracy, introduced by the approximation of boundary conditions and the method employed for computing state variable derivatives, and refines the mesh accordingly is viewed as a better approach for the reduction of computational cost. The solution of a boundary value problem arising in interface contact conditions involves surface integration, which is carried out over the element surface rather than the actual tool surface. When linear elements are used with a curved die, the interface as represented by elements in contact is always smaller than the actual contact area. For deformation processes that are sensitive to friction and thickness of material, this type of error could be serious. Increasing the number of elements at the contact boundary can help in minimising error. Incorporation of adaptive mesh refinement in which the mesh is automatically refined in areas of sharp stress gradient will also help. Finite element analysis of cup drawing in the presence of friction is due to Haluk and Atan (1996). A finite element solution incorporating Coulomb friction has been proposed by Dalin and Onate (1989). A concept based on the insertion of a fictitious intermediate layer between the tool and blank for the contact modelling was presented by Doege, Kaminsky, and Bagaviev (1999). Most recovery procedures used in adaptive techniques are based on

*Corresponding author. Email: moahmed@kku.edu.sa

the least square fitting of velocity (or the displacement) field or their derivatives (stress field) by a higher order polynomial over an elemental or nodal patch. Zienkiewicz and Zhu (1987) discussed error estimation procedures based on recovery techniques and their effectiveness in linear problems. A velocity-based recovery technique has been presented by Singh, Sekhon, and Shishodia (1999). The optimisation study of adaptive mesh refinement during finite element simulation has been carried out by Ahmed, Sekhon, and Singh (2005). Selman, Meinders, Boogaard van den, and Huétink (2003) has predicted wrinkling in sheet metal forming using error indicators based on proposed combination of element thickness and geometrical error. An adaptive numerical analysis for deep drawing process has been carried out by Cherouat, Giraud-Moreau, and Borouchaki (2007). Chung, Kim, Lee, Ryu, and Joun (2014) has presented three-dimensional finite element analysis of sheet metal forming process employing solid element remeshing procedures and effect of single and double layer of mesh on deformed shape and thickness variation of cold sheet forming process is studied. In this paper, the effect of interfacial contact on the adaptive mesh refinement during simulation of the axisymmetric cup drawing operation considering frictional and non-friction contact on different sheet thicknesses has been investigated.

2. Finite element formulation

During the drawing operation, the material is subjected to large strains. Therefore, the material may be assumed to behave as a rigid plastic or rigid visco-plastic material. The flow formulation (Zienkiewicz, 1984) may be adopted to arrive at the finite element equations. It requires that among all admissible velocity fields u_i that satisfy the conditions of compatibility and incompressibility, as well as the velocity boundary conditions, the actual solution extremalises the following functional.

$$\pi = \int_V \bar{\sigma}\dot{\bar{\varepsilon}}\ \mathrm{d}V - \int_{sf} F_i u_i\ \mathrm{d}S \tag{1}$$

where $\bar{\sigma}$ is the effective stress, $\dot{\bar{\varepsilon}}$ is the effective strain rate and F_i represents surface tractions.

Expressing Equation (1) in terms of equivalent stress, equivalent strain and imposing the incompressibility constraint by introducing the penalty term, the following relationship is obtained (Kobayashi, Oh, & Altan, 1989).

$$\delta\pi = \int_V \bar{\sigma}\delta\dot{\bar{\varepsilon}}\ \mathrm{d}V + K\int_s \dot{\varepsilon}_v\delta\dot{\varepsilon}_v\ \mathrm{d}V - \int_{sf} F_i\delta u_i\ \mathrm{d}S = 0 \tag{2}$$

where K, a penalty constant, is a large positive constant of the order of $(10^6$–$10^8)\ \mu$

where $\mu = \frac{\bar{\sigma}}{3\dot{\bar{\varepsilon}}}$

Equation (2) may be discretised in terms of nodal point velocities v_i of different elements and their variation δV. From the arbitrariness of δv_i, the following set of algebraic equations is obtained.

$$\frac{\partial\pi}{\partial v_i} = \sum_J \left(\frac{\partial\pi}{\partial v_i}\right)_{(J)} = 0 \tag{3}$$

where upper case suffix 'J' indicates that the marked quantity pertains to the Jth element and the lower-case suffix 'i' refers to the nodal point number 'i'. Equation (3) is obtained by evaluating $\partial\pi/\partial V_i$ at the elemental level and assembling them into the global equation under appropriate constraints.

Equation (3) can be simplified and expressed in the following form.

$$\boldsymbol{K} \cdot \boldsymbol{\delta V} = \boldsymbol{f} \tag{4}$$

where $\boldsymbol{K}$ is called the stiffness matrix and $\boldsymbol{f}$ is the residual of the nodal point force vector.

The magnitude of the frictional stress at a point on the blank is dependent on the magnitude of the relative sliding velocity u_s between the blank and the die. The direction of the frictional stress f_s and relative sliding velocity u_s is opposite to each other. The relationship between f_s and u_s may be expressed as follows.

$$f_s = -m\,k\,\frac{u_s}{\|u_0\|} \cong -m\,k\,\left(\frac{2}{\pi}\tan^{-1}\left[\frac{u_s}{u_0}\right]\right) \tag{5}$$

where u_0 is a small threshold velocity.

3. Treatment of contact

During metal forming operations, contact conditions at the blank and tool boundaries continuously change. New nodes may come in contact with the tool and some of the existing nodes may lose contact with the tool during successive time steps. If assume $\boldsymbol{v^0} = \boldsymbol{v_0}$, where $\boldsymbol{v^0}$ is the initial value of the velocity field for the next increment and $\boldsymbol{v_0}$ is the computed velocity field at the end of the previous time increment. Let $\boldsymbol{x^0} = \boldsymbol{x_0} + \Delta \boldsymbol{t}\ \boldsymbol{v_0}$, where $\boldsymbol{x^0}$ corresponds to the co-ordinates of a material points $\boldsymbol{m^0}$ (the initial mesh for the next increment) and $\boldsymbol{x_0}$ corresponds to those in the previous mesh $\boldsymbol{m_0}$.

If $\boldsymbol{m^0}$ is an inner point, put $\boldsymbol{x} = \boldsymbol{x^0}$. If point $\boldsymbol{x} = \boldsymbol{x_0}$ stays a free boundary point or a sliding contact point, then the boundary condition is unchanged, $\boldsymbol{x} = \boldsymbol{x^0}$. If $\boldsymbol{m^0}$ penetrates the tool, then the boundary condition becomes a sliding contact condition which needs modification of time increment. Instead of projecting $\boldsymbol{m^0}$ on to the tool boundary, the time increment can be adjusted such that $\boldsymbol{m^0}$ just lies on the tool boundary. For this purpose, the following relationship may be used.

$$\Delta \boldsymbol{t}^* = \frac{\boldsymbol{d}_0}{(\boldsymbol{v}_0 - \boldsymbol{v}_t) \cdot \boldsymbol{n}} \tag{6}$$

where $\boldsymbol{d_0}$ is the distance between $\boldsymbol{m^0}$ and the tool boundary along the normal n to the boundary segment. $\boldsymbol{x^0}$ is recalculated using modified time increment $\boldsymbol{x^0} = \boldsymbol{x_0} + \Delta \boldsymbol{t}^*\ \boldsymbol{v_0}$. Tangential component of velocity $\boldsymbol{v_t}$ at $\boldsymbol{m^0}$ is calculated from $\boldsymbol{v_0}$ and set equal to $(\boldsymbol{v_0}.\ \boldsymbol{t})$ where $\boldsymbol{t}$ is the tangential vector.

4. Illustrative example

An adaptive finite element code AdSheet2 was specifically developed for the simulation of deep drawing operations (Figure 1). The von-Mises yield criterion has been employed. The material of the sheet is modelled as rigid plastic. The friction at die-metal interface is modelled through a constant factor in which frictional stress is related to shear strength of the material. The punch and die are considered as rigid. The die and blank interface can be modelled as sliding friction or sticking friction. The direct approach has been adopted for contact analysis wherein the contacting nodes are

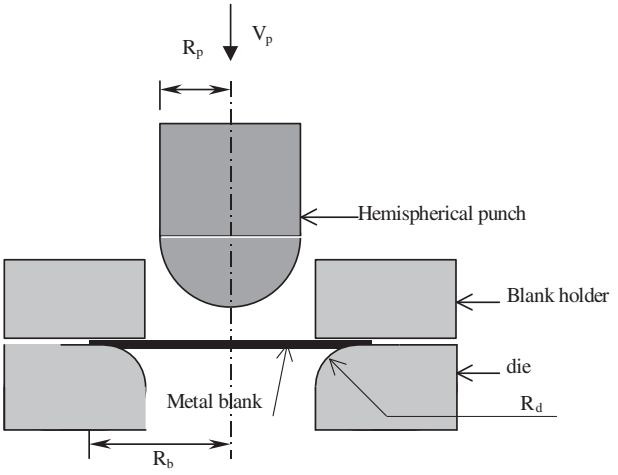

Figure 1. Schematic diagram of deep drawing operation.

constrained in the normal direction of tool surface, and frictional boundary condition is imposed directly. The displacement of punch is modelled in incremental steps. Each displacement increment was such that it caused a maximum strain increment of 1%. Velocity recovery-based adaptive finite element procedures have been implemented in the above code. The velocity smoothing was carried on a patch of elements surrounding the element under consideration. The error was estimated in the energy norm. The strategy adopted for adaptive mesh refinement was the error equally distributed. The validation of the developed code is given in the published literature (Ahmed & Singh, 2008). Due to symmetry, only one-half of the blank was modelled. The code was used to simulate the examples of axisymmetric deep drawing operation by a hemispherical punch in the presence of non-frictional and frictional contact at die-blank interface of different thickness. The blank is discretised using six nodded triangular elements. The input parameters were as follows.

Radius of Blank and Punch, $R_b = 66.0$ mm; $R_p = 50.8$ mm; Blank-holder Pressure = 5 kN; Velocity of Punch $V = 1$ mm/s; Mesh size reduction factor = 1.2; Target error = 8%,

$$\text{Stress–strain relation} \bar{\sigma} = 589[0.0001 + \bar{\varepsilon}]^{0.216}$$

where $\bar{\sigma}$ and $\bar{\varepsilon}$ are effective stress and effective strain, respectively.

Three cases of sheet thickness, namely, 1, 2 and 3 mm with three values of friction factors, namely, .0, .15 and .3 at sheet contact were considered. Although the analysis provides detailed numerical results for each time increments, the variations in mesh at only two stages of deformation, namely, initial and final, are studied. The sheet blank is divided into three regions for discussion purpose. Region I is the portion of the blank between centre of blank and a point up to which the punch is in contact with the blank, region II corresponds to the portion of the blank neither in contact with punch nor with the die or blank holder and region III corresponds to the portion of the blank which is in contact with the die and the blank holder. The computed mesh and deformed shapes at punch displacement of 2.5 and 25.0 mm are shown in figures from Figures 3 to 8 for different friction factor and sheet thickness.

5. Results and discussion

5.1. *Effect of sheet thickness*

A user-defined uniform mesh was used at the beginning of the adaptive analysis for 1 mm with two layers and for 2 and 3 mm thick sheet with four layers of elements (Figure 2). The value of friction factor considered in each case of sheet thickness is .3. The number of elements in the case of blanks of thickness, 1, 2 and 3 mm was 590, 828 and 752, respectively (Figure 2). The corresponding degrees of freedom were 2910, 3770 and 3382 respectively. For 1 and 2 mm thickness of the blank, two remeshings were needed to keep the error below the target limit of 8%. A total of four remeshings were required in the case of blank of 3 mm thickness. The CPU time needed for analysis for 1, 2 and 3 mm sheet was 9 h 45 min, 4 h and 3 h, respectively. The non-adaptive analysis considering the uniform mesh throughout the deformation for sheet thickness of 1 mm has also been carried out. The CPU time needed for non-adaptive analysis was 3 h only. The meshes and deformed shapes at punch displacements of 2.5 and 25.0 mm corresponding to various thickness of the sheet are shown in Figure 3–5. The number of elements and degrees of freedom of the refined mesh, in case of 1 mm thickness of blank were 2230 and 9810 at a punch displacement of 2.5 mm. The corresponding numbers rose to 1200 and 5390, respectively, at a punch travel of 25.0 mm. The number of elements and corresponding degrees of freedom, in case of 2 mm thick sheet were 1443 and 6232 at punch displacement of 2.5 mm, and 995 and 4384, respectively, at punch displacement of 25.0 mm. The refined mesh in the 3 mm thick blank consisted of 1634 elements and 7006 degrees of freedom at a punch displacement of 2.5 mm and, 1602 elements and 6856 degrees of freedom at 25.0 mm punch displacement.

The mesh and deformed shapes at punch displacement of 2.5 and 25.0 mm in the three cases of thickness are shown in Figures 3–5. It is visible from the mesh plot, with increase in deformation, the high-density mesh of centre portion move away from the centre. The movement of denser mesh after adaptive remeshing is more in case of lower thickness of sheet as compared to the higher thickness. It can also be observed

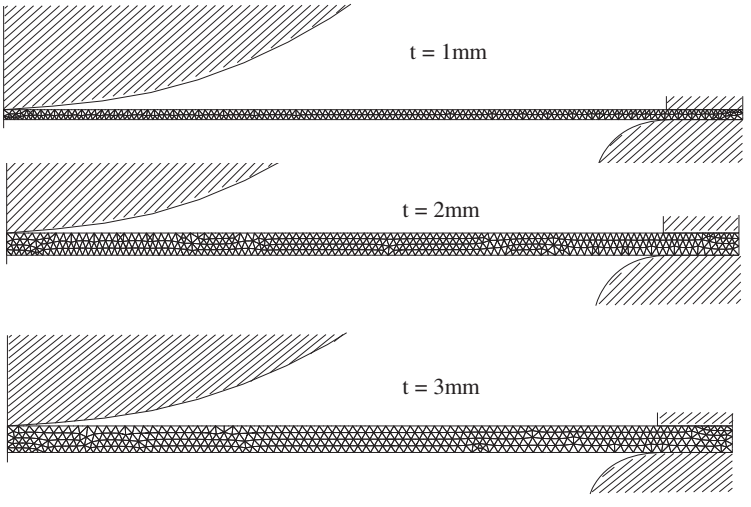

Figure 2. Uniform mesh for thickness (*t*).

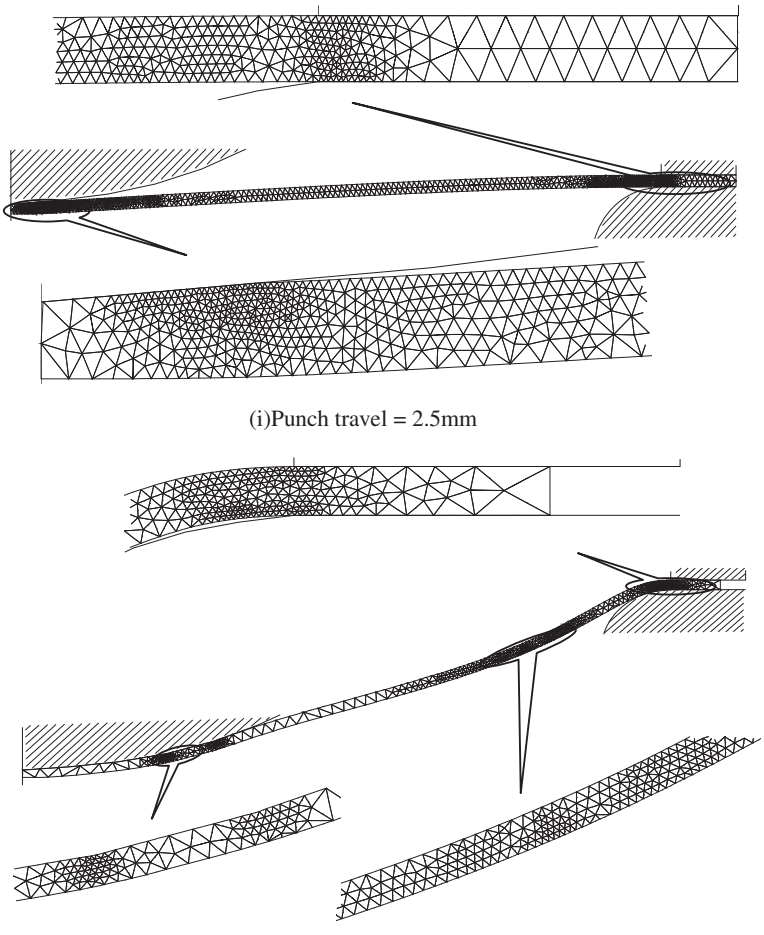

(i)Punch travel = 2.5mm

(ii)Punch travel = 25.0mm

Figure 3. Mesh and deformed shape (thickness = 1.0 mm, $f = .3$).

from the mesh plots that after adaptive remeshing, the density of elements in some portion of the sheet becomes high as the blank comes under the contact of punch or die. For example, in the case of 1 mm thickness of blank, mesh of the blank portion that is in contact with punch or die become very fine. Figure 3 (i) shows that the mesh of region I at punch displacement of 2.5 mm has finer elements having 11 layers of elements. Also, the very fine mesh of this region of sheet is on contact face and relatively coarse mesh on the free bottom face. At same displacement of punch, region III also has nine layers of elements. As this region has contact condition at both faces, the high-density mesh is developed throughout the sheet thickness. Region II continues to have more or less a uniform coarse mesh except at the end zones. The distribution of element at a punch displacement of 25.0 mm is, however, quite different. The region I now has very coarse mesh except at edge of contacting punch. The middle portion of region II shows high-density of elements near the die portion but other part of region II has very low-density mesh. The region III has finer elements in the vicinity of interface of die radius with the blank and coarser elements in the blank along the straight portion of die.

The mesh in the case of blank of 2 mm thickness at punch displacement of 2.5 mm shows that the density of elements in regions I and III is high with similar distribution of mesh as in the mesh of 1 mm thick sheet (Figure 4). The end of the region II adjacent to regions I and III has high element density. The density decreases towards the central portion of region II that has more or less a uniformly coarse mesh. The mesh at a punch displacement of 25.0 mm indicates that high-density zone of region I is located in the vicinity of the outer edge of punch. The elements of region II may be divided into two zones. The zone near region I has a coarse mesh while the zone near region

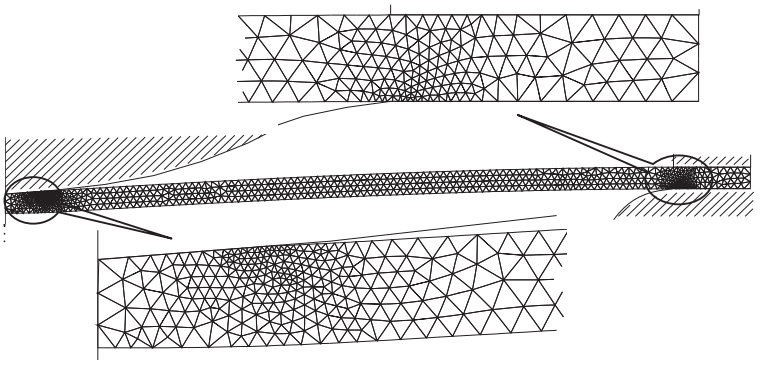

(i)Punch travel = 2.5mm

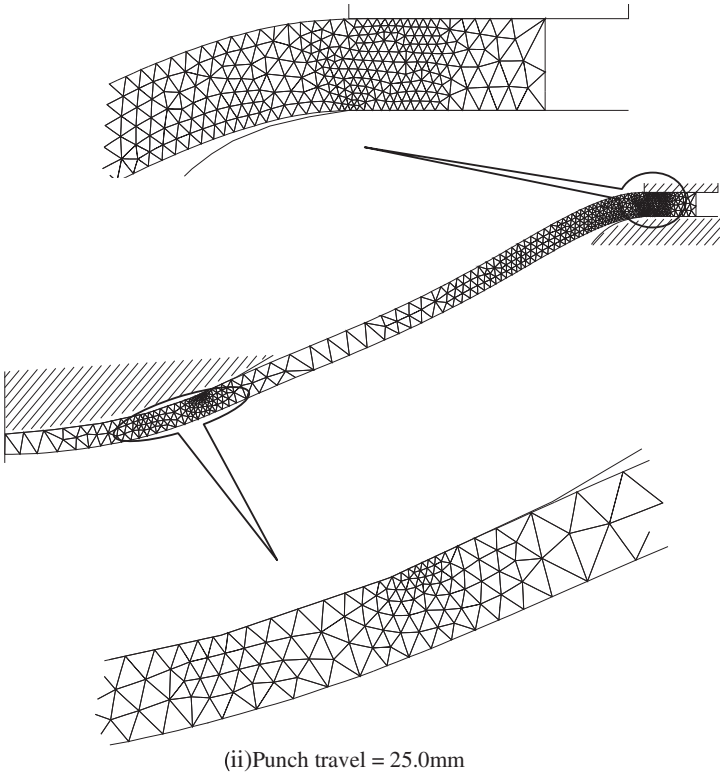

(ii)Punch travel = 25.0mm

Figure 4. Mesh and deformed shape (thickness = 2.0 mm, $f = .3$).

III consists of a finer mesh. Because of contact condition on both faces, mesh refinement develops a fine mesh throughout the thickness in region III except at the outer end edge of straight portion of die where coarser elements are formed.

The element distribution in the 3 mm thick sheet at a punch displacement of 2.5 mm (Figure 5) exhibits that whole region I has finer elements having unstructured mesh and the density of elements decreases towards the bottom of sheet. Region II has finer elements around its ends and a uniformly coarse mesh in the central portion. The portion of the blank adjoining the die radius of region III has high density of elements but the mesh density decreases towards the top of sheet. The mesh at a punch displacement of 25.0 mm indicates that region I has finer elements throughout the sheet thickness. However, the fineness slightly decreases towards the bottom surface. The face contact condition is not seemed to affects the refinement in this region. Region II has a mesh density more of less similar to the original uniform mesh. The whole of the region III has fine elements. The highest element density, however, is found around the start of die radius i.e. at the contact of blank and die.

Tables 1–3 list the peak values of effective strain, effective stress in the sheet and computed punch load at different stages of deformation corresponding to different

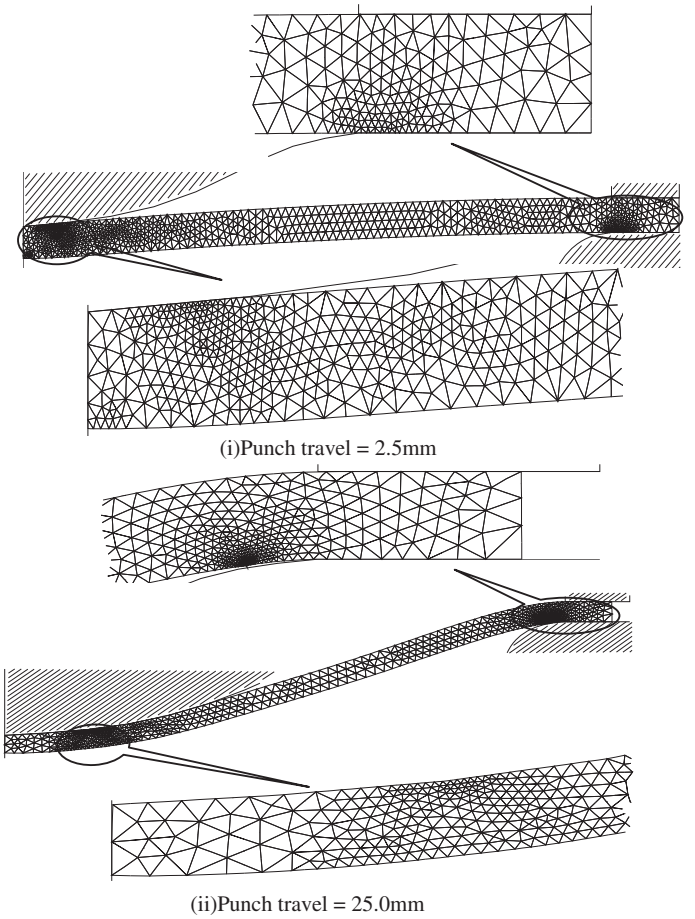

Figure 5. Mesh and deformed shape (thickness = 3.0 mm, $f = .3$).

Table 1. Peak values of effective strain, effective stress and punch load (blank thickness, $h = 1.0$ mm).

Punch displacement (mm)	Effective strain	Effective stress (N/mm^2)	Punch load (kN)
2.5	.421891	488.86	.56
10.0	.445108	494.55	5.26
15.0	.482974	503.35	9.21
20.0	.534975	507.43	12.87
25.0	.654932	512.14	15.7

Table 2. Peak values of effective strain, effective stress and punch load ($h = 2.0$ mm).

Punch displacement (mm)	Effective strain	Effective stress (N/mm^2)	Punch load (kN)
2.5	.425316	516.12	1.92
10.0	.471597	958.95	13.88
15.0	.490920	1013.78	20.92
20.0	.710906	1039.38	29.92
25.0	.769290	1077.57	36.10

Table 3. Peak values of effective strain, effective stress and punch load ($h = 3.0$ mm).

Punch displacement (mm)	Effective strain	Effective stress (N/mm^2)	Punch load (kN)
2.5	.450044	495.72	4.49
10.0	.470820	500.58	20.60
15.0	1.915191	677.76	34.79
20.0	2.228335	700.74	45.18
25.0	2.434623	756.46	54.50

thicknesses of sheet. It is inferred from the tables that the magnitudes of effective strain increase with increase in punch displacement. For example, the peak values of effective strain at punch displacements of 2.5 and 25.0 mm are .421891 and .654932, respectively, for 1 mm sheet thickness. The peak effective strain values for 1 mm thickness of blank are smaller than those corresponding to 2 and 3 mm thickness of blank. For example, the peak values of effective strain at punch displacement of 2.5 and 25.0 mm are .425316 and .769290, and .450044 and 2.434623 respectively for 2 and 3 mm thickness of sheet.

From the tables, it is observed that peak effective stress increases with increase in sheet deformation. In reference to the three thicknesses considered, the peak value of effective stress for 1 mm thickness of blank is lesser as compared to the peak effective strain values of 2 and 3 mm thickness at all stages of deformation. The peak effective stress values of 2 mm thickness are higher as compared to the values for 3 mm sheet thickness. The peak effective stress at punch displacement of 2.5 and 25.0 mm is (488.86 and 512.14 N/mm^2), (516.12 and 1077.57 N/mm^2) and (495.72 and 756.46 N/mm^2), respectively, for 1, 2 and 3 mm thickness of sheet. It is also observed from the tables that as anticipated the punch load increases with increase in punch displacement and also with the increase in thickness of sheet. The increase in punch load in early stages of displacement is less as compared to the latter stages of displacement.

Table 4. Peak value of effective strain and punch load at different stages of deformation using non-adaptive and adaptive analysis (for $h = 1$ mm and $f = .3$).

	Non-adaptive		Adaptive	
Punch displacement (mm)	Effective strain	Punch load (kN)	Effective strain	Punch load (kN)
2.5	.421891	.55	.421891	.56
10.0	.432341	5.25	.445108	5.26
15.0	.446573	9.05	.482974	9.21
20.0	.462411	13.39	.534975	12.87
25.0	.484542	17.17	.654932	15.7

The magnitudes of punch load at final punch displacement are 14.7, 35.1 and 54.5 kN for 1, 2 and 3 mm sheet thickness, respectively.

The results of adaptive analysis and non-adaptive analysis having uniform meshing are also compared. Table 4 depicts the peak value of effective strain and punch load obtained from the adaptive and non-adaptive analysis for sheet thickness of 1 mm and friction factor of .3. The table shows that the peak effective strain values employing uniform meshing are smaller than those corresponding to adaptive analysis. The peak values of effective strain at punch displacements of 2.5 and 25.0 mm are .421891 and .654932, respectively, obtained with adaptive analysis while at similar deformation with non-adaptive analysis, the peak values of effective strain are .421891 and .484542. The table also predicts that there is no significant effect of adaptive refinement on punch load.

5.2. Effect of friction factor

For the study of effect of frictional contact conditions on deep drawing process, 2 m thick sheet blank with different friction factor is adopted. At the start of the analysis, a user-defined uniform mesh consisting of 828 elements with 3770 degrees of freedom was generated in each case of friction factors (Figure 2). Only one remeshing occurred in cases of friction factor of .0 and .15. However, four remeshing were required in case of friction factors of .3. The CPU time of analysis was more or less same for all values of friction factor. The meshes and deformed shapes at punch displacements of 2.5 mm, 25.0 mm corresponding to different friction factors are shown in Figures 6–8. From the mesh plots, it can be seen that after adaptive remeshing, the initially uniform mesh got adaptively refined (i.e. the refinement of elements occurred in some portions of the blank and coarsening of elements in other portions). The refined mesh in the frictionless case consisted of 1372 elements and 6034 degrees of freedom. The corresponding values in the case of friction factor of .15 were 1356 elements and 5970, respectively. The refined mesh in the case of friction factor of .3 at different punch displacement was different at different amount of punch displacement. At punch displacement of 2.5 mm, the number of elements and degrees of freedom were 1443 and 6232, respectively. The corresponding values at a punch displacement of 25.0 mm were 995 and 4394, respectively. The meshes and deformed shapes at punch displacements of 2.5 mm, 25.0 mm corresponding to various friction factors are shown in Figures 6–8. From the mesh plots, it can be seen that adaptive remeshing refines the initially uniform mesh into one of variable density.

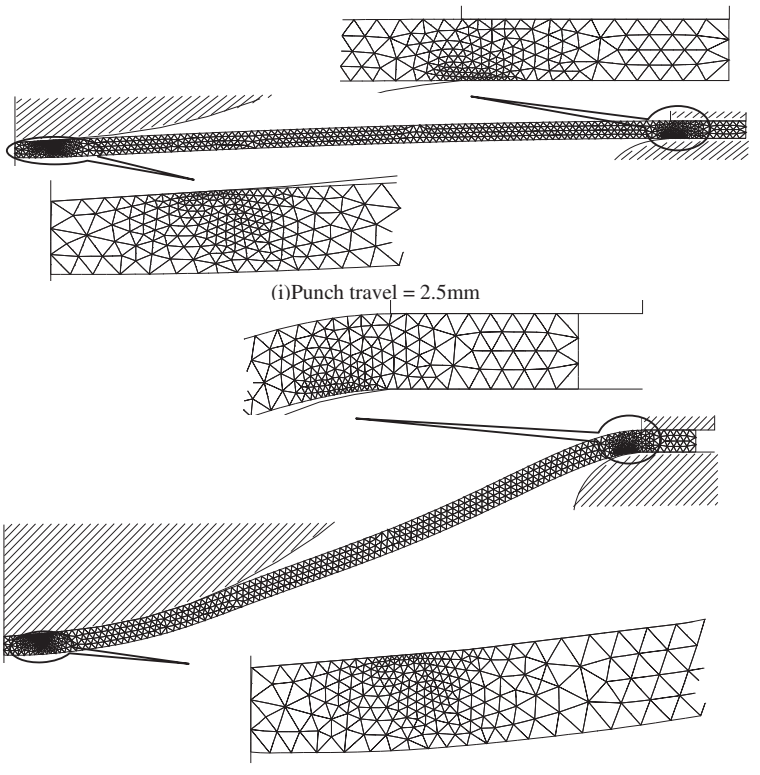

Figure 6. Mesh and deformed shape (friction factor = .00, t = 2 mm).

The mesh obtained at a punch displacement of 2.5 mm in the frictionless case (Figure 6) shows that the density of elements in region I is high. The mesh density decreases towards the centre of the blank and towards the bottom of sheet. The end of the region II adjoining region I has high element that tends to decrease towards the central portion of region II. This portion of region II adjoining has more or less a uniformly coarse mesh. In region III, the density of elements is greater in the vicinity of the inner peripheries of die-blank and blank holder-blank interfaces. The elements are finer at interface of the die-blank as compared to the blank holder-blank interface. The rest of the portion of region III has coarser elements. At a punch displacement of 25.0 mm, the middle portion of region I has high mesh density. Region II has uniformly coarse elements throughout. The elements of region III are finer in the vicinity of the inner peripheries of die-blank interface. The mesh density tends to decrease towards the top of the sheet. In the straight portion along the die, a uniform but coarse mesh is generated.

Figure 7 depicts that the distributions of elements in the deformed mesh at different amounts of punch displacement corresponding to f = .15 are similar to the corresponding distributions in the frictionless case.

The refined mesh for .3 friction factor and punch displacement of 2.5 mm (Figure 8) show that a highly dense mesh is generated in region I. The density decreases towards

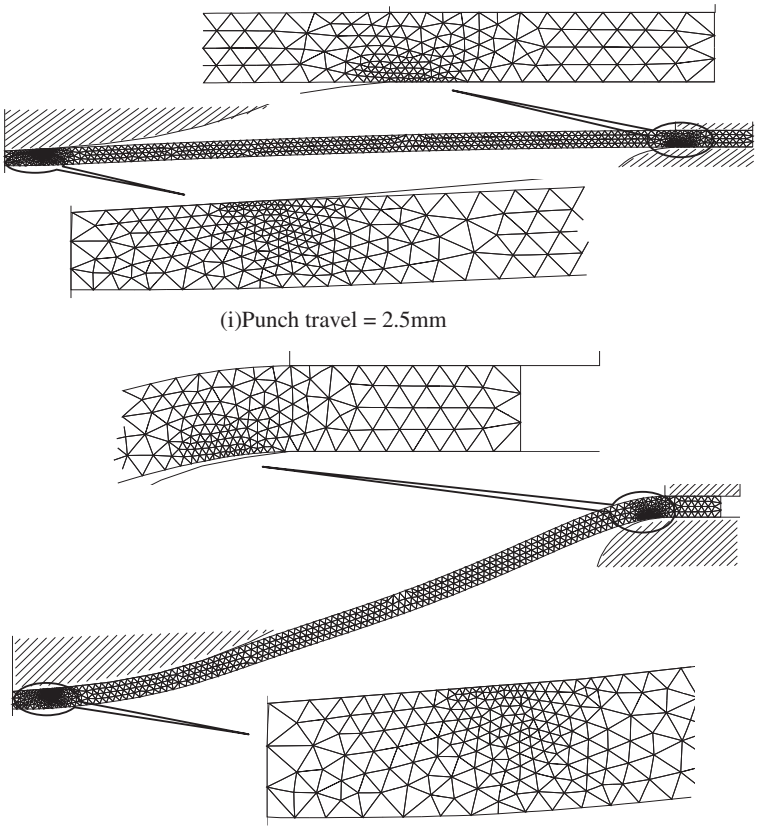

(i)Punch travel = 2.5mm

(ii)Punch travel = 25.0mm

Figure 7. Mesh and deformed shape (friction factor = .15, t = 2 mm).

the centre of the blank and towards the bottom of the sheet. A uniform coarser mesh is generated in region II. In region III, the density of elements is greater at the inner interface of the die-blank. The mesh density decreases towards the top surface of the sheet. At a punch displacement of 25.0 mm, portion of region I situated near the centre of blank has very coarse mesh but the portion away from the centre has relatively fine elements. Region II has coarser elements at the end adjoining region II and fine element at the end adjoining region III. The whole of region III has fine elements throughout the thickness except in the outer straight portion. The fineness of elements in region III decreases towards the top of the blank sheet. It can be concluded that at high-frictional conditions, the adaptive refined mesh is markedly different form the mesh at non-friction or low-friction contact conditions.

Tables 5–7 show the relationship of effective strain, effective stress and punch load at different stages of deformation for various values of friction factor. It is inferred from the tables that the magnitudes of effective strain increase with increase in punch displacement. Tables show that with lower frictional conditions, there is no effect on peak effective strain and effective stress at different punch displacement. However, with increasing the friction factor, the peak effective strain increases at all stages of

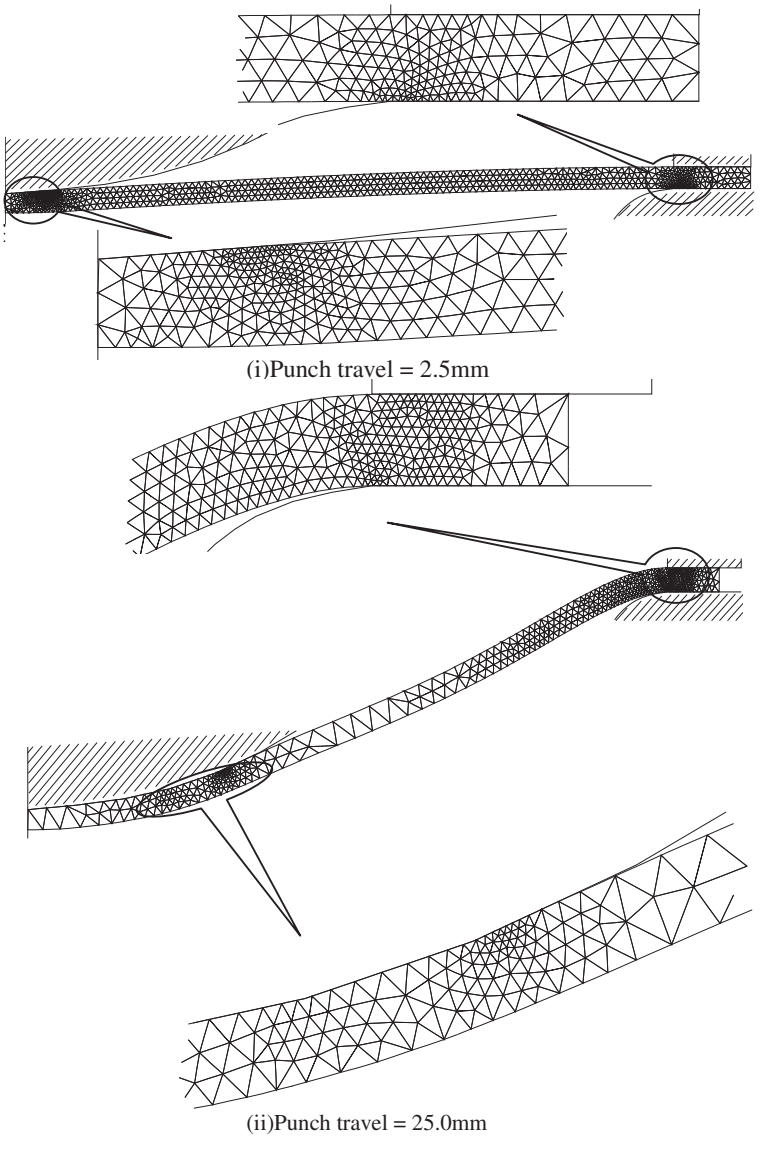

Figure 8. Mesh and deformed shape (friction factor = .30, t = 2 mm).

deformations. For example, the peak values of effective strain at punch displacement of 2.5 and 25.0 mm are (.425315 and .648413), (.425315 and .647145) and (.450044 and 2.434623), respectively, with friction factors .0, .15 and .3. It is also seen from the tables that the effective stress increases at all stages of deformations with increasing the friction factor except at intermediate level of friction. At intermediate friction level, the peak effective stress increases in the beginning of deformations and decreases with further increase in the deformation. It is observed from the tables that as anticipated the punch load increases with increase in punch displacement. Also the punch load is not significantly affected by variations in frictional factor. The magnitudes of punch load at considered punch displacement are about 35 kN with all frictional conditions.

Table 5. Peak values of effective strain, effective stress and punch load (friction factor, $f = .0$ mm).

Punch displacement (mm)	Effective strain	Effective stress (N/mm^2)	Punch load (kN)
2.5	.425315	489.71	2.01
10.0	.463196	498.82	12.35
15.0	.519078	511.24	20.95
20.0	.568216	521.32	29.68
25.0	.648413	534.32	36.31

Table 6. Peak values of effective strain, effective stress and punch load ($f = .15$ mm).

Punch displacement (mm)	Effective strain	Effective stress (N/mm^2)	Punch load (kN)
2.5	.425315	489.71	1.96
10.0	.463529	807.85	12.36
15.0	.518,694	935.47	20.95
20.0	.561,141	519.91	29.94
25.0	.647,145	531.32	36.17

Table 7. Peak values effective strain, effective stress and punch load ($f = .30$ mm).

Punch displacement (mm)	Effective strain	Effective stress (N/mm^2	Punch load (kN)
2.5	.425316	516.12	1.92
10.0	.471597	958.95	13.88
15.0	.490920	1013.78	20.92
20.0	.710906	1039.38	29.92
25.0	.769290	1077.57	36.10

6. Conclusion

A study of adaptive mesh refinement during the deep drawing operation under different contact condition of variable thickness of blank has been carried out. Three different cases of friction factors and sheet thickness have been analysed. The finite element analysis method coupled with adaptive refinement procedure refines the mesh in zones of contact locations. The non-adaptive study having uniform mesh throughout the deformation has also been carried out to compare with the adaptively refined mesh analysis. The efficiency of a non-adaptive analysis is higher as compared to the adaptive analysis. From the mesh plots of adaptively refined mesh, it is found that an initial uniform mesh of deep drawing having different frictional condition and different thickness becomes non-uniform or refined after regeneration whenever the error of the solution exceeds the predefined limit.

Two remeshings were needed to keep the error below the target limit for lower thickness of the blank and four remeshings were required in the case of higher blank thickness. In the first regeneration, the number of elements is increased but with further regeneration, the number of elements is found to decrease with all considered thickness. The non-uniform mesh with high-density zones is different at different stages of deformation. The finer element zone moves gradually away from the centre of the blank with increase in deformation. The movement of high-density zone is more pronounced at lower sheet thickness. The CPU time for process simulation decreases with increase

of sheet thickness. The magnitudes of effective strain and effective stress increase with increase in deformation and blank thickness. The punch load increases with the increase in thickness of sheet. The increase in punch load in early stages of displacement is more as compared to the latter stages of displacement with different thickness.

Only a single remeshing is needed at smaller values of the friction factor. However, greater numbers of remeshings are required for higher values of the friction factor to achieve the target accuracy. The distribution of elements is substantially similar at different stages of deformation for lower friction factors. But mesh distribution is different at different stages of deformation in case of higher values of the friction factor. The CPU time of simulation remains approximately unaffected by values of the friction factor. The effective strain and effective stress increase with increase in deformation and frictional factors. The punch load is not significantly affected when the friction factor is changed over a wide range.

References

Ahmed, M., Sekhon, G. S., & Singh, D. (2005). Developments in the finite element simulation of sheet metal forming processes. *Defence Science Journal, 55*, 29–42.

Ahmed, M., & Singh, D. (2008). An adaptive parametric study on mesh refinement during adaptive finite element simulation of sheet forming operations. *Turkish Journal of Engineering and Environmental Sciences, 32*, 163–175.

Cherouat, A., Giraud-Moreau, L., & Borouchaki, H. (2007). Adaptive refinement procedure for sheet metal forming, Proceedings 9th International Conference NUMIFORM'07, *AIP Conference Proceedings*. *908*, 937–942. Porto.

Chung, W., Kim, B., Lee, S., Ryu, H., & Joun, M. (2014). Finite element simulation of plate or sheet metal forming processes using tetrahedral MINI-elements. *Journal of Mechanical Science and Technology, 28*, 237–243.

Dalin, J. B., & Onate, E. (1989). An automatic algorithm for contact problems, application to sheet metal. In A. Samuelsson, E. G. Thompson, R. D. Wood, & O. C. Zienkiewicz (Eds.), *Numiform'89, numerical in industrial methods forming processes* (pp. 419–424). Rotterdam: CRC Press.

Doege, E., Kaminsky, C., & Bagaviev, A. (1999). A new concept for the description of surface friction phenomena. *Journal of Materials Processing Technology, 94*, 189–192.

Haluk, D., & Atan, T. (1996). Analysis of axisymmetric cup drawing in relation to friction. *Journal of Materials Processing Technology, 58*, 293–301.

Kobayashi, S., Oh, S., & Altan, T. (1989). *Metal forming and the Finite Element Method*. New York, NY: Oxford University Press.

Selman, A., Meinders, T., Boogaard van den, A. H., & Huétink, J. (2003). Adaptive numerical analysis of wrinkling in sheet metal forming. *International Journal of Forming Processes, 6*, 87–102.

Singh, D., Sekhon, G. S., & Shishodia, K. S. (1999). *Finite element analysis of metal forming processes with error estimation and adaptive mesh generation*. Proceedings of 11th ISME Conference (pp. 616–621). New Delhi.

Zienkiewicz, O.C. (1984). Flow formulation for numerical solution of forming processes. In J. F. T. Pitman, O. C. Zienkiewicz, R. D. Wood, & J. M. Alexander (Eds.), *Numerical analysis of forming processes* (pp. 1–44). Chichester: Wiley.

Zienkiewicz, O. C., & Zhu, J. Z. (1987). A simple error estimator and adaptive procedure for practical engineering analysis. *International Journal for Numerical Methods in Engineering, 24*, 335–357.